

Supplementary Materials for
Brightening deep-blue perovskite light-emitting diodes: A path to Rec. 2020

Seungjae Lee *et al.*

Corresponding author: Jung-Yong Lee, jungyong.lee@kaist.ac.kr

Sci. Adv. **10**, eadn8465 (2024)
DOI: 10.1126/sciadv.adn8465

This PDF file includes:

Figs. S1 to S14
Table S1

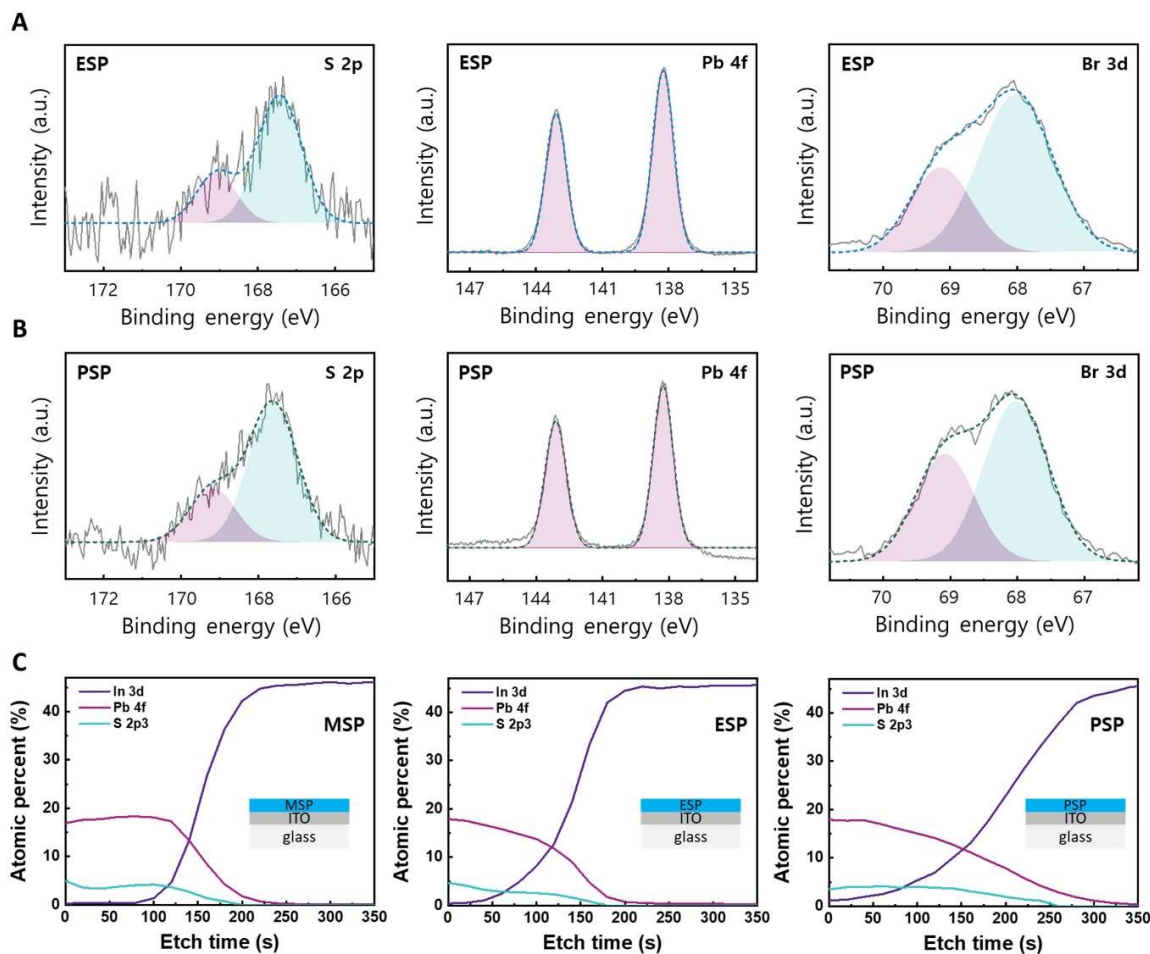


Fig. S1. Verification of bonding between sulfonate ligands and perovskite. (A-B) X-ray photoelectron spectroscopy (XPS) spectra corresponding to S 2p, Pb 4f, Br 3d for (A) ethanesulfonate-treated perovskite (ESP) film, and (B) propanesulfonate-treated perovskite (PSP) film. (C) XPS depth profiles of methanesulfonate-treated perovskite (MSP), ESP, and PSP films.

Fig. S1 demonstrates the successful bonding of ethanesulfonate and propanesulfonate with a perovskite material. Particularly, S 2p peaks composed of $\text{SO}_3\text{-C}$ and Pb-O-S can be observed in both ethanesulfonate-treated perovskite (ESP) and propanesulfonate-treated perovskite (PSP) films, as opposed to the control perovskite (CP) where the S 2p peaks are not visible (36). The presence of S 2p for ESP and PSP provides evidence of the successful incorporation of ethane- and propanesulfonate ligands into the perovskite structure. The binding energies of Pb 4f^{5/2} and Pb 4f^{3/2} for ESP and PSP, at 142.9 and 138.1 eV, are lower than those of CP, at 143.3 and 138.5 eV (38). Moreover, the absence of metallic lead (Pb^0) peaks can be noted for ESP and PSP, whereas such peaks were observed in CP films (37).

These results suggest that the sulfonate ligands passivated lead ions effectively. Furthermore, the lower Br 3d binding energies of ESP (68.0 and 69.2 eV) and PSP (68.0 and 69.2 eV), compared to CP, also indicate the incorporation of sulfonate ligands (40).

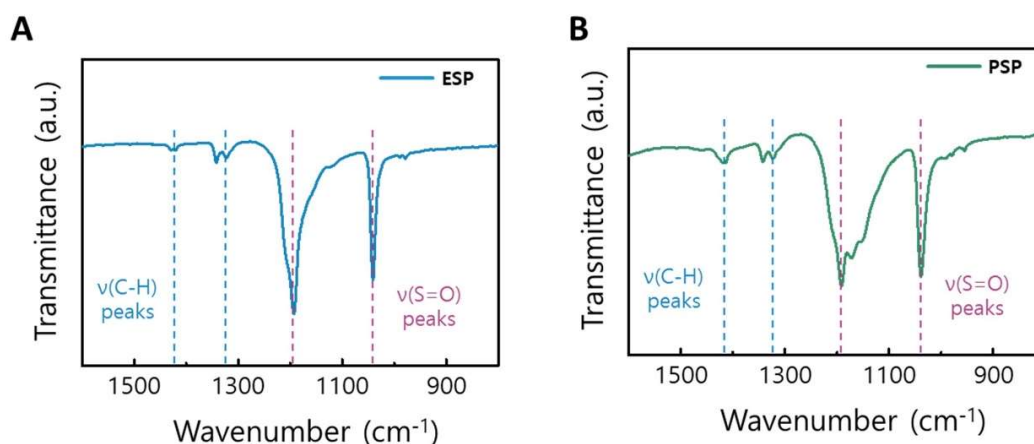


Fig. S2. Confirmation of the presence of sulfonate ligands within the films. Fourier-transform infrared spectroscopy (FT-IR) spectrum for (A) ESP, and (B) PSP.

As shown in Fig. S2, Alkane bending vibration ($\nu(\text{C-H})$), ranging from 1365 to 1470 cm^{-1} , and S=O stretching vibration ($\nu(\text{S=O})$), within the range of 1130 to 1250 cm^{-1} , were observed in both ESP and PSP (41). The presence of alkane bending vibration and S=O stretching vibration peaks confirms the existence of sulfonate ligands in the ESP and PSP films.

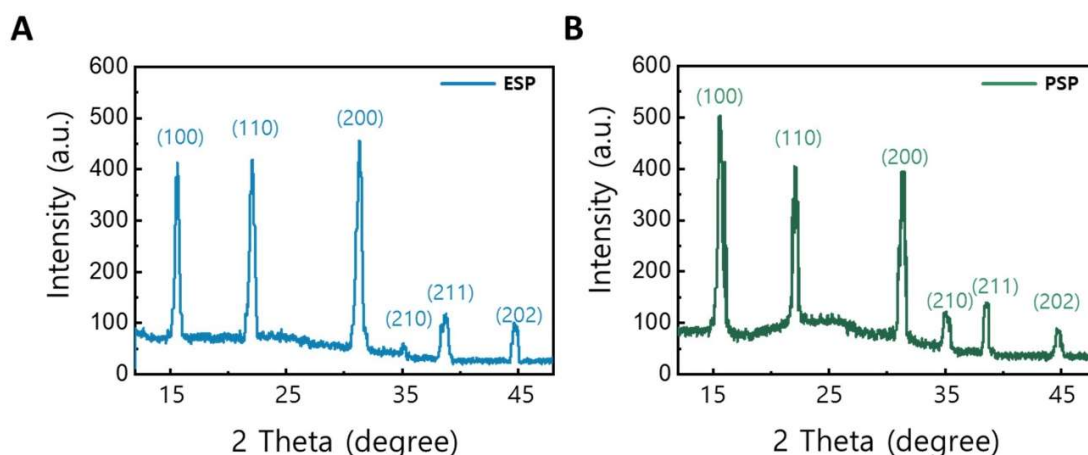


Fig. S3. Crystallographic analysis of sulfonate ligands-treated films. X-ray diffraction (XRD) patterns of (A) ESP, and (B) PSP.

Fig. S3 demonstrates that X-ray diffraction (XRD) patterns of ESP and PSP suggest that the backbone chain length of the sulfonate ligands did not induce changes in crystallographic phases (42,43,45). Similar to methanesulfonate, the incorporation of both ethanesulfonate and propanesulfonate with the perovskite structure did not alter the cubic phase.

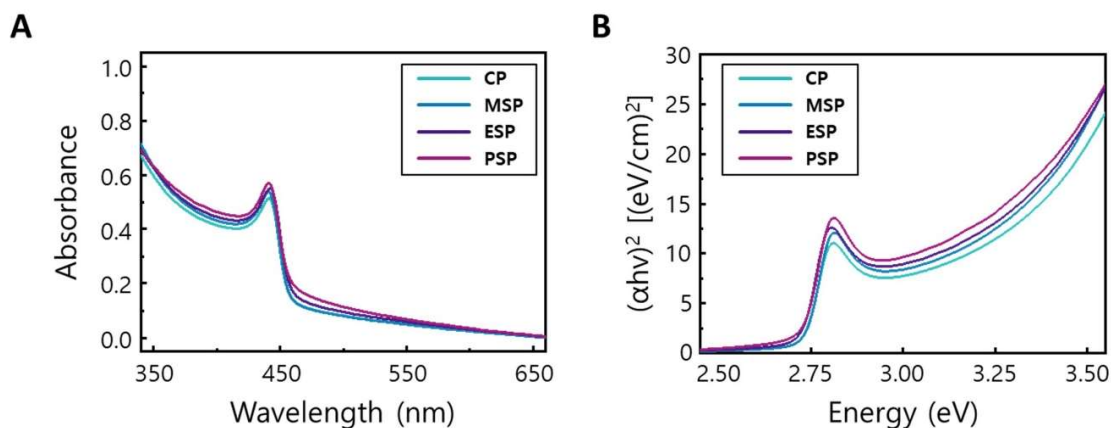


Fig. S4. Absorption properties exhibited by various samples. (A-B) (A) Ultraviolet-visible (UV-vis) absorption spectra and (B) Tauc plot of control perovskite (CP), MSP, ESP, and PSP films.

As shown in Fig. S4, CP, methanesulfonate-treated perovskite (MSP), ESP, and PSP films displayed absorption spectra without any additional peaks below 450 nm. These results suggest that the methanesulfonate, ethanesulfonate, and propanesulfonate ligands did not induce the formation of 2-dimensional (2D) structures (47,48).

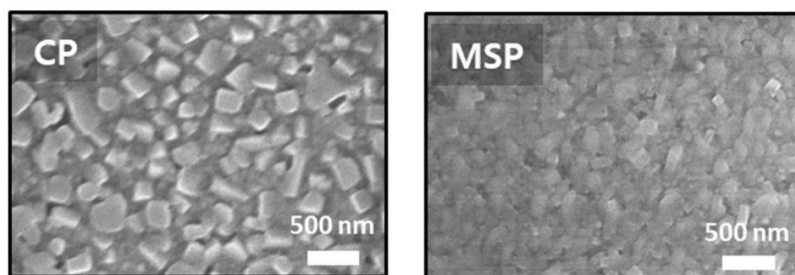


Fig. S5. Morphological changes resulting from the incorporation of sulfonate ligands. Scanning electron microscopy (SEM) images of CP and MSP films.

The implementation of MS ligands as observed in the scanning electron microscopy (SEM) images (Fig. S5), resulted in a notable decrease in grain size, reducing it from an initial size of approximately 300 nm to 120 nm.

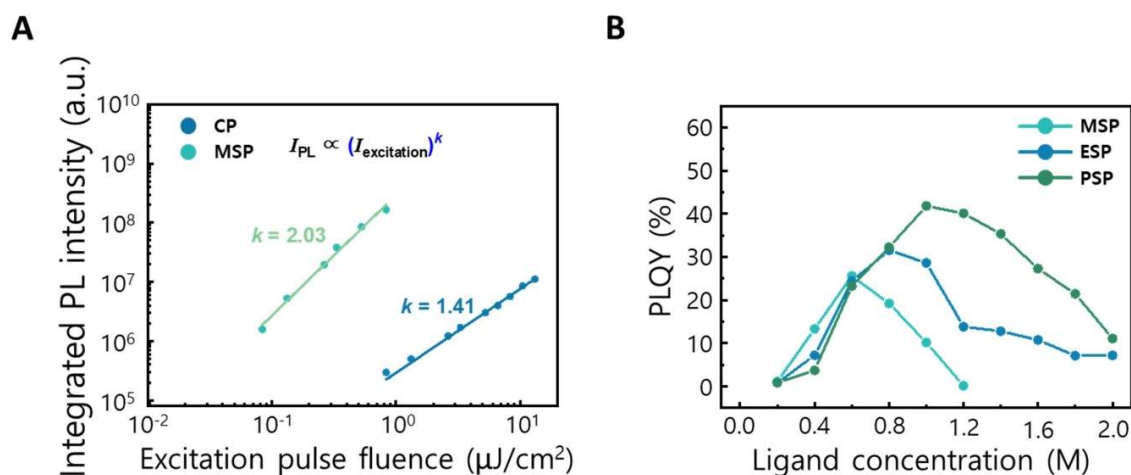


Fig. S6. Photoluminescence properties exhibited by the films. (A) Power dependent photoluminescence analysis for CP and MSP. **(B)** Photoluminescence quantum efficiency (PLQY) of MSP, ESP, and PSP with different concentrations of 3 different ligands.

Fig. S6A illustrates the degree of bimolecular recombination. The MSP films, with a k value of 2.03, show a higher bimolecular-type recombination possibility than CP films, which have a k value of 1.41. Fig. S6B illustrates the photoluminescence quantum yield (PLQY) variations corresponding to the concentration of three distinct ligands: MSP, ESP, and PSP. Optimal PLQY values are observed at methane-, ethane-, and propanesulfonate/Pb(II) ratios of 0.6, 0.8, and 1.0, respectively. As the carbon chain length increases from methane to propane, maximum PLQY values are enhanced: 25.6% for MSP, 31.6%; PSP, 41.8%.

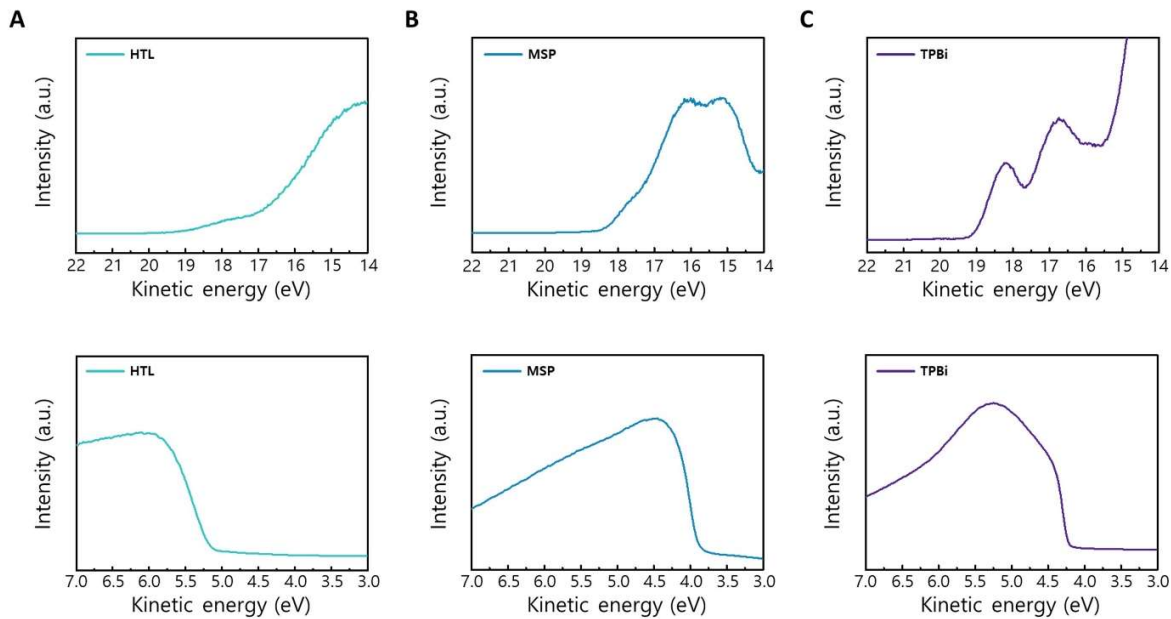


Fig. S7. Ultraviolet photoelectron spectroscopy of different layers. Ultraviolet photoelectron spectroscopy (UPS) of (A) hole-transporting layer (HTL), (B) MSP and (C) 2,2',2''-(1,3,5-Benzinetriyl)-tris(1-phenyl-1-H-benzimidazole) (TPBi).

Fig. S7 shows the spectra of ultraviolet photoelectron spectroscopy (UPS), which was employed to determine the energy levels of three materials: hole-transporting layer (HTL), MSP, and 2,2',2''-(1,3,5-Benzinetriyl)-tris(1-phenyl-1-H-benzimidazole) (TPBi). The work function values for hole-transporting layer (HTL), MSP, and TPBi were found to be 5.2, 3.9, and 4.2 eV, respectively. Additionally, the energies corresponding to the valence band edge for MSP, and TPBi were found to be 7.2, 6.6, and 6.4 eV, respectively.

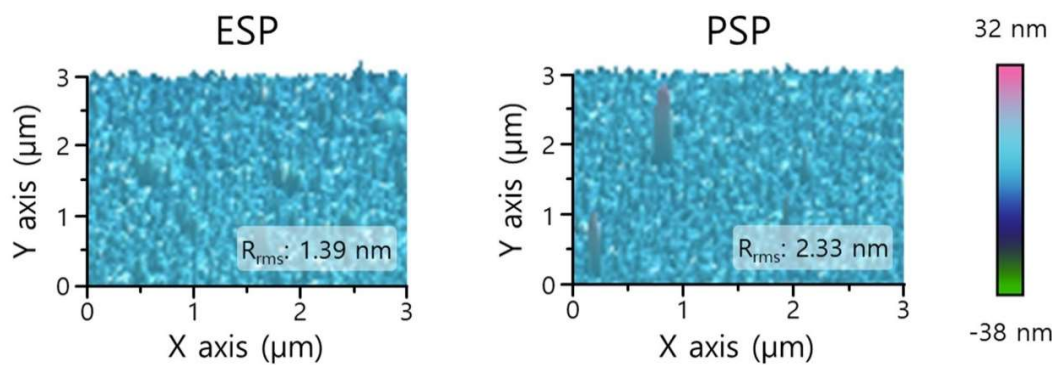


Fig. S8. Morphological changes induced by the different ligands. Atomic force microscopy (AFM) images and roughness analysis for ESP and PSP films.

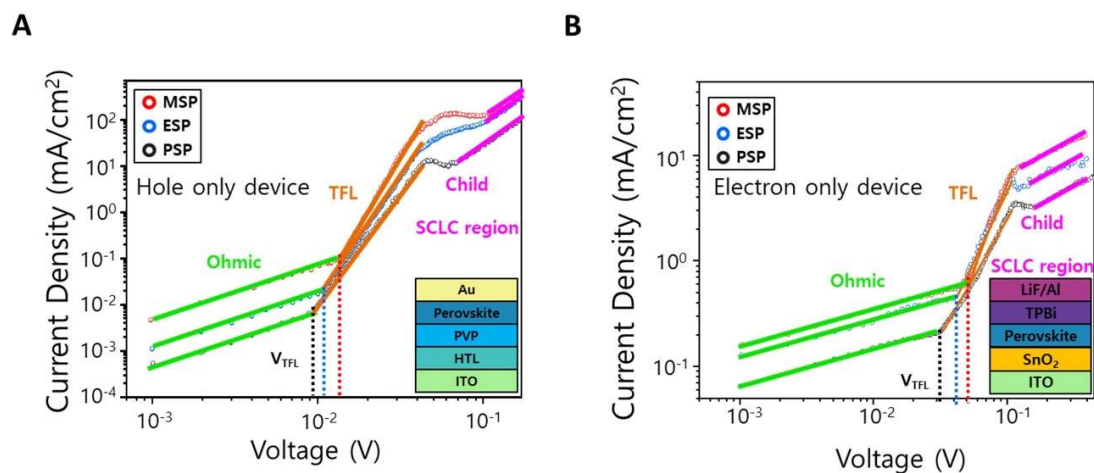


Fig. S9. Electrical characterizations of single carrier devices with distinct active layers. Current density (J)-voltage (V) curves of MSP, ESP, and PSP-used single carrier devices (**A**) hole-only devices with a device structure of indium tin oxide (ITO)/ HTL/PVP/Perovskite/Au, and (**B**) electron-only devices with a device structure of ITO/tin oxide (SnO_2)/Perovskite/TPBi/lithium fluoride (LiF)/Al.

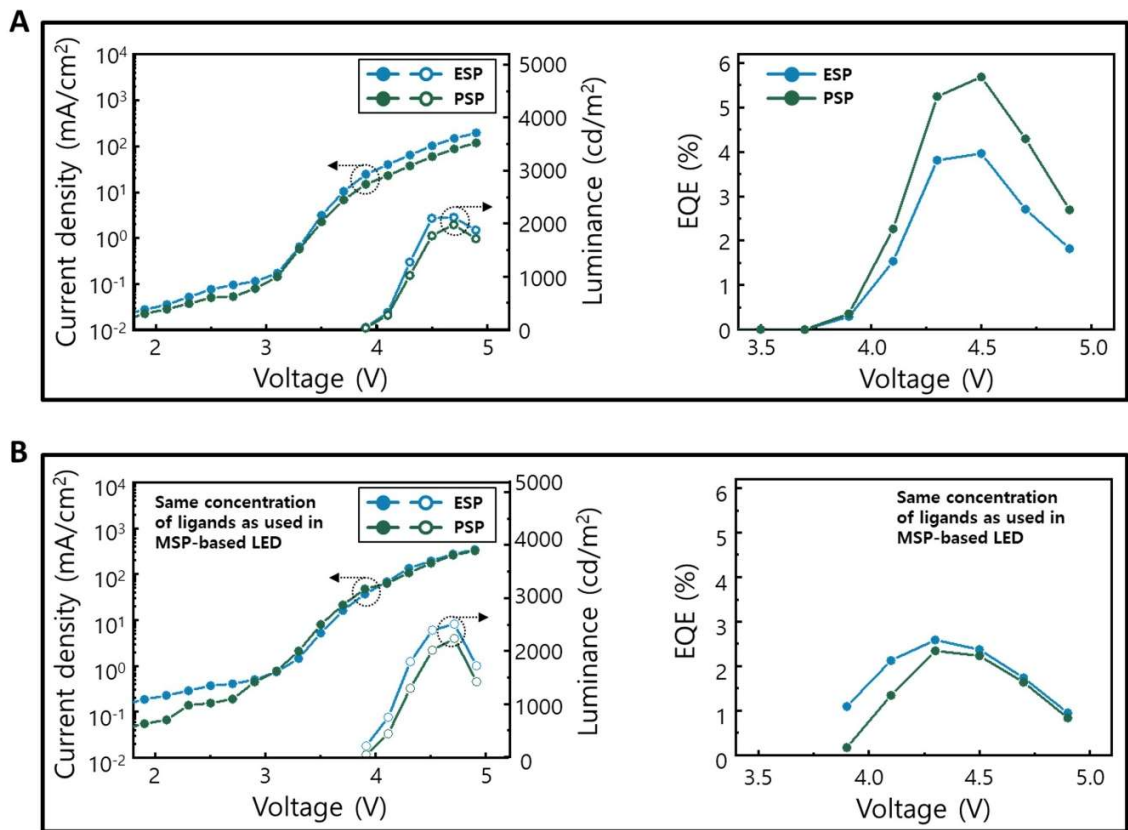


Fig. S10. Comparison of performances of the devices with different emission layers. (A) Performance characteristics of ESP and PSP-based light emitting diodes (LEDs), showing their current density and luminance, and external quantum efficiency (EQE). **(B)** Performances of ESP and PSP-based LEDs with the same concentration of ligands as utilized in the MSP-based LED.

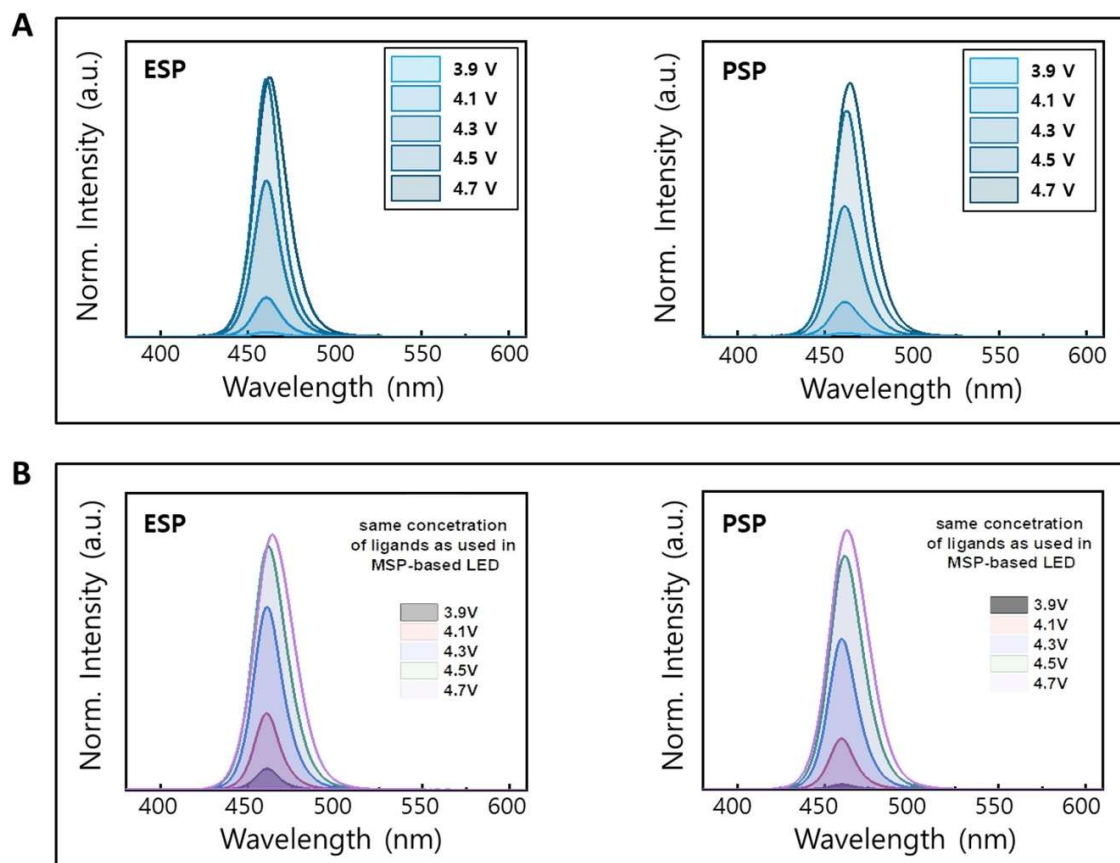


Fig. S11. Spectral stability of the devices with different emission layers. (A) Electroluminescence (EL) spectra of ESP-based LED and PSP-based LED at different driving voltages. **(B)** EL spectra of ESP- and PSP-based LEDs with the same concentration of ligands as used in MSP-based LED at different driving voltages.

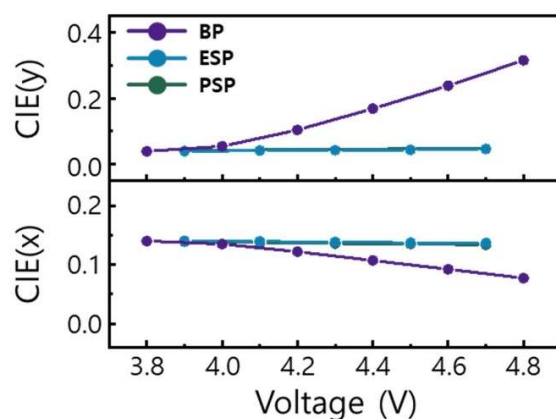


Fig. S12. Comparison of spectral stability among various devices. Variations in Commission Internationale de l'Éclairage (CIE) x- and y-coordinates under different operating voltages for perovskite light-emitting diodes (PeLEDs) constructed from CP, ESP and PSP

LED operation stability at
initial luminance of 100 cd/m²

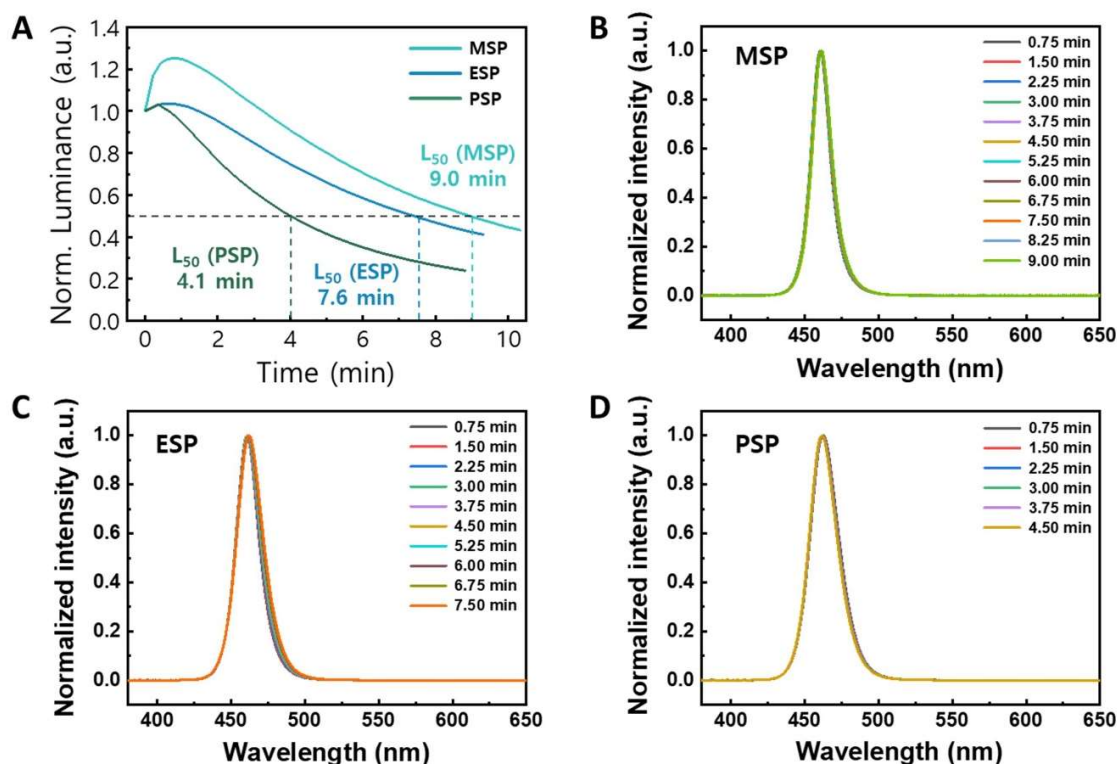


Fig. S13. Operational lifetimes and spectral stability under a constant voltage. (A) Operational lifetimes of MSP, ESP, and PSP-based LEDs at the initial luminance of 100 cd/m². (B-D) EL spectra over time of (B) MSP-, (C) ESP-, and (D) PSP-based LEDs

Compared to MSP film (0.93 nm), the surface roughness of ESP and PSP films was slightly higher: 1.39 nm for ESP, 2.33 nm for PSP (Fig. S8). Notably, perovskite grains were not uniformly formed in ESP and PSP films, exhibiting pointed shapes that became more pronounced with longer carbon chains (Fig. S8). This rise in roughness contributes to a higher density of grain boundaries, negatively affecting color stability and operational lifespan (Figs. S11-S13). Despite their slightly rougher surfaces and decreased charge carrier mobilities (Figs. S8, S9 and Table S1), ESP- and PSP-based LEDs achieved higher external quantum efficiencies (EQE) of 3.96% and 5.68%, respectively, compared to MSP-based PeLED (Fig. S10). Furthermore, Table S1 shows that PSP, which exhibits higher PLQY, has a lower trap density than ESP and MSP in single carrier devices. Conversely, decreased charge carrier mobilities resulted in lower luminance for ESP- and PSP-based PeLEDs of 2,489 and 1,978 cd/m², respectively (Figs. S9, S10 and Table S1).

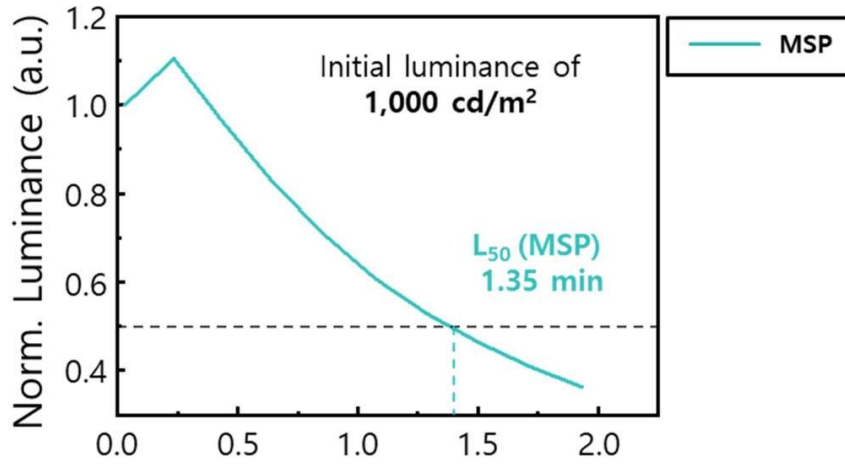


Fig. S14. Operating lifespan under high brightness conditions. Operational lifetimes of MSP-based LEDs at the initial luminance of 1,000 cd/m².

Table S1. Parameters obtained from single carrier devices. Trap density, hole and electron mobilities derived from space charge limited current (SCLC) measurement in single carrier devices.

	MSP	ESP	PSP
N_t [cm⁻³]	4.443 × 10¹⁴	3.614 × 10¹⁴	2.951 × 10¹⁴
Electron mobility [cm²V⁻¹s⁻¹]	6.57 × 10⁻⁴	4.03 × 10⁻⁴	2.18 × 10⁻⁴
Hole mobility [cm²V⁻¹s⁻¹]	1.51 × 10⁻³	1.06 × 10⁻³	3.89 × 10⁻⁴